Cancer Research

miR-21 Inhibition Reduces Liver Fibrosis and Prevents Tumor Development by Inducing Apoptosis of CD24$^+$ Progenitor Cells

Jing Zhang[1], Jingjing Jiao[1], Silvia Cermelli[2], Kyle Muir[2], Kwang Hwa Jung[1], Ruhai Zou[1,3], Asif Rashid[4], Mihai Gagea[5], Sonya Zabludoff[6], Raghu Kalluri[7], and Laura Beretta[1,2]

Abstract

miR-21 is upregulated in hepatocellular carcinoma and intrahepatic cholangiocarcinoma, where it is associated with poor prognosis. Here, we offer preclinical evidence that miR-21 offers a therapeutic and chemopreventive target in these liver cancers. In mice with hepatic deletion of *Pten*, anti-miR-21 treatment reduced liver tumor growth and prevented tumor development. These effects were accompanied with a decrease in liver fibrosis and a concomitant reduction of CD24$^+$ liver progenitor cells and S100A4$^+$ cancer-associated stromal cells. *Notch2* inhibition also occurred in tumors following anti-miR-21 treatment. We further showed that miR-21 is necessary for the survival of CD24$^+$ progenitor cells, a cellular phenotype mediated by Notch2, osteopontin, and integrin αv. Our results identify miR-21 as a key regulator of tumor-initiating cell survival, malignant development, and growth in liver cancer, highlighting the role of CD24$^+$ cells in the expansion of S100A4$^+$ cancer-associated stromal cells and associated liver fibrosis. *Cancer Res; 75(9); 1859–67. ©2015 AACR.*

Introduction

miRNA are small noncoding RNA molecules that affect mRNA stability and translation by targeting the 3′-untranslated region (3′-UTR) of various transcripts. Dysregulation of miRNAs affects a wide range of cellular processes, including cell proliferation and differentiation. Interest in miRNA-21 (miR-21) has increased recently, especially in cancer and cardiovascular diseases (1). miR-21 is upregulated in almost all types of cancers, promotes cancer cell proliferation, migration, and survival and therefore was classified as an onco-miR (2, 3). High levels of miR-21 are often associated with aggressive forms of cancer and poor patient survival. miR-21 is significantly upregulated in hepatocellular carcinoma (HCC) and is associated with poor prognosis (4–10). miR-21 was also reported to be overexpressed in intrahepatic cholangiocarcinoma and cholangiocarcinoma, but no correlation with clinicopathological features was found (10, 11). A role of miR-21 in organ fibrosis has also been described (1). miR-21 regulates epithelial-to-mesenchymal transition (EMT), a process in which fibroblasts derive from epithelial or endothelial cells, resulting in organ fibrosis. A direct evidence for a role of miR-21 in organ fibrosis was obtained from studies in mouse models of cardiac and pulmonary fibrosis (12, 13). Upregulation of miR-21 was found in human fibrotic livers, resulting in chronic hepatitis C virus (HCV) infection and intrahepatic miR-21 levels positively correlated with HCV viral load, fibrosis severity, or serum liver transaminase levels (14). Cirrhosis, the result of end-stage fibrosis, is a common preneoplastic condition associated with hepatocarcinogenesis (15). It is therefore highly relevant to study the role of miR-21 in hepatocarcinogenesis. Deletion of the PI3K/PTEN in hepatocytes leads to steatohepatitis, fibrosis, hepatocyte dysplasia, and HCC later in life, reproducing the steps of HCC development observed in human HCC (16, 17). It therefore represents an excellent model to evaluate the potential of targeting miR-21 for the treatment and chemoprevention of HCC.

Materials and Methods

Mice treatment

C57BL/6 mice carrying *Pten* conditional knockout alleles were crossed with an *Albumin (Alb)-Cre*-transgenic mouse. For this model, control animals are *Pten*$^{loxP/loxP}$; *Alb-Cre*$^-$ while the experimental mice *are Pten*$^{loxP/loxP}$; *Alb-Cre*$^+$. Only male mice were included in this study as female mice develop tumors at a much lower incidence rate. Two separate sets of treatment were performed. In the first set, 12 × 10.5-month-old male *Pten*-null mice received anti-miR-21 (25 mg/kg) in PBS carriage medium or placebo by intraperitoneal injection. In the second set, 12 × 7.5-month-old male *Pten*-null mice received anti-miR-21 (25 mg/kg) or placebo by intraperitoneal injection. The anti-miR-21

[1]Department of Molecular and Cellular Oncology, The University of Texas MD Anderson Cancer Center, Houston, Texas. [2]Molecular Diagnostics Program, Public Health Sciences Division, Fred Hutchinson Cancer Research Center, Seattle, Washington. [3]State Key Laboratory of Oncology in Southern China, Department of Ultrasound, Sun Yat-sen University Cancer Center, Guangzhou, P.R. China. [4]Department of Pathology, The University of Texas MD Anderson Cancer Center, Houston, Texas. [5]Department of Veterinary Medicine and Surgery, The University of Texas MD Anderson Cancer Center, Houston, Texas. [6]Regulus Therapeutics, Inc, San Diego, California. [7]Department of Cancer Biology, The University of Texas MD Anderson Cancer Center, Houston, Texas.

Note: Supplementary data for this article are available at Cancer Research Online (http://cancerres.aacrjournals.org/).

Corresponding Author: Laura Beretta, Department of Molecular and Cellular Oncology, The University of Texas MD Anderson Cancer Center, 1515 Holcombe Boulevard, Houston, TX 77030. Phone: 713-792-9100; Fax: 713-794-4023; E-mail: lberetta@mdanderson.org

doi: 10.1158/0008-5472.CAN-14-1254

used was a high-affinity oligonucleotide complementary to the active site of miR-21 with a phosphorothioate backbone containing modifications (DNA, MOE, cET; Regulus Therapeutics). The PK of these chimeric phosphorothioate antisense oligonucleotides is independent of the sequence. The compounds PK and pharmacodynamics across species (mice, primates, human) together with their safety profiles and dose-dependent actions in liver, the major organ of deposition, have been described (18). All mice received eight injections over a period of 6 weeks, three injections in the first week of treatment and one injection per week in the following 5 weeks. C57BL/6 wild-type (wt) and OPN knockout ($OPN^{-/-}$) mice were purchased from The Jackson Laboratory. A total of 7 × 10-week-old male wt mice and 6 × 10-week-old male $OPN^{-/-}$ mice were fed with either normal diet or a diet supplemented with 0.1% diethoxycarbonyl-1, 4-dihydro-collidin (DDC; Sigma-Aldrich) for 4 weeks. All animal studies were carried out in strict accordance with institutional regulations and every effort was made to minimize the number of animals required for the study and to minimize the pain and discomfort experienced.

miR-21 *in situ* hybridization and immunofluorescence costaining

Formalin-fixed paraffin-embedded tissue sections were deparaffinized in xylene, and rehydrated using ethanol dilutions. For miR-21 in situ hybridization, tissue sections were digested with 5 μg/mL proteinase K for 5 minutes at room temperature, then loaded onto Ventana Discovery Ultra for in situ hybridization analysis. The tissue slides were incubated with double-DIG labeled mercury LNA microRNA probe (Exiqon) for 2 hours at 55°C. The digoxigenins were then detected with a polyclonal anti-DIG antibody and alkaline phosphatase conjugated second antibody (Ventana) using NBT-BCIP as the substrate. Negative miRNA probe from Exiqon was used as negative control. Positive control was performed using miRNA U6. For costaining, miRNA probe labeled slides were treated with 3% H_2O_2 to inactivate endogenous peroxidase and blocked with 5% BSA in PBS (w/v). OPN (R&D) primary antibody was used followed by secondary antibody incubation in PBST and tyramine-conjugated fluorochrome.

Apoptosis assays

In vitro cell apoptosis was tested using FITC Annexin V Apoptosis Detection Kit (BD Pharmingen) following transfection with 20 nmol/L oligonucleotide (hsa-miR-21 Anti-miR from Ambion Life Technologies) for 72 hours using 10 μL Lipofectamine RNAiMAX transfection reagent. For OPN rescue assays, 1 μg/mL of recombinant OPN protein (R&D) was added to the culture medium following anti-miR-21 transfection. For ITGAV blocking experiments, 5 μg/mL of ITGAV-blocking antibody (Abcam) was added to the culture medium. Same amount of IgG was used as negative control.

Additional methods are provided in Supplementary Methods.

Results

In mice with hepatocytic deletion of *Pten*, miR-21 expression is increased in liver tumors, correlates with fibrosis in adjacent liver, and is enriched in progenitor cells

Hepatic deletion of *Pten* in male mice induced liver steatosis at around 3 months and steatosis severity increased with aging, remaining stable after 6 month (Supplementary Fig. S1A). Mild liver fibrosis was detected in 6-month-old *Pten*-null mice and gradually increased in severity with aging (Supplementary Fig. S1B). At 9-month-old, around 80% of the *Pten*-null mice had developed tumors and all 12-month-old mice presented with tumors (Supplementary Fig. S1C). We measured the expression of miR-21 in the liver and tumors of these mice. miR-21 levels were not statistically different in control healthy liver and in steatotic liver from 6-month-old *Pten*-null mice (median of 3.7×10^9 copies and 2.9×10^9 copies, respectively). miR-21 expression significantly increased in liver of 9- and 12-month-old *Pten*-null mice (median $= 7.99 \times 10^9$ copies, $P < 0.001$) and further increased in tumors (median $= 13.0 \times 10^9$ copies, $P = 0.02$; Fig. 1A). Fibrosis and lipid depositions were measured by histology in all mice and the size of the tumors was recorded. Although levels of miR-21 did not correlate with tumor size or steatosis levels, miR-21 expression strongly correlated with fibrosis severity ($R = 0.71$; Fig. 1B).

By *in situ* hybridization of miR-21 in liver and tumors of *Pten*-null mice, we did not detect any miR-21 expression in hepatocytes nor HCC cells. Instead, a strong positive miR-21 signal was detected in ductular reaction areas in the liver, in areas surrounding the tumors and in neoplastic biliary cells (Fig. 1C). More specifically, miR-21 was enriched in cells expressing osteopontin (OPN, Spp-1), a marker of hepatic progenitor cells and biliary cells (Fig. 1D). To further validate the relevance of this expression pattern in human disease, *in situ* hybridization of miR-21 was performed on six human resected HCCs. As observed in the *Pten*-null mouse model, miR-21 was mainly expressed in areas surrounding the tumors and in non-neoplastic bile ducts. The tumor areas were negative in five HCCs and partially positive in the sixth one (Fig. 1E).

Anti-miR-21 treatment inhibits tumor growth, modifies the tumor differentiation phenotype, and reduces liver fibrosis

To evaluate the therapeutic potential of targeting miR-21, we treated 10.5-month-old *Pten*-null mice for 6 weeks, with chemically modified antisense oligonucleotides specific for miR-21. At necropsy, tumors and adjacent tissues were collected and processed for gene expression and histology analyses. We first validated the anti-miR-21 treatment efficiency by measuring miR-21 target genes *Sprouty-1* and *Sprouty-2* (*Spry1* and *Spry2*). Upon anti-miR-21 treatment, expression of *Spry1* and *Spry2* significantly increased (2.1-fold; $P = 0.032$ and 2.0-fold; $P = 0.043$, respectively), confirming that the anti-miR-21 treatment was effective in reducing miR-21 activity (Fig. 2A). We next evaluated the effect of anti-miR-21 on tumor growth (Fig. 2B–D). Anti-miR-21 treatment decreased the ratio of liver/body weight from 23.4% to 20.1% ($P = 0.028$; Fig. 2B). Although anti-miR-21 treatment did not affect the average number of tumors per mouse (2.7 and 2.8 for placebo and anti-miR-21 groups, respectively; Fig. 2B), the average tumor burden in anti-miR-21 treated mice was significantly smaller than in placebo-treated mice (891 mm^3 compared with 2,308 mm^3, $P = 0.05$; Fig. 2C). The average tumor size in anti-miR-21 treated mice was also significantly smaller than that in placebo-treated mice (342 mm^3 compared with 865 mm^3, $P = 0.05$; Fig. 2C). The reduction in tumor size following anti-miR-21 treatment was further demonstrated by the tumor size distribution per mouse in both groups. While half of the tumors in placebo-treated mice were >500 mm^3, only 21.7% of the tumors in anti-miR-21 treated mice were >500 mm^3 (Fig. 2D).

Blinded evaluation by a pathologist of 14 tumors from the placebo group and 11 tumors from the anti-miR-21-treated

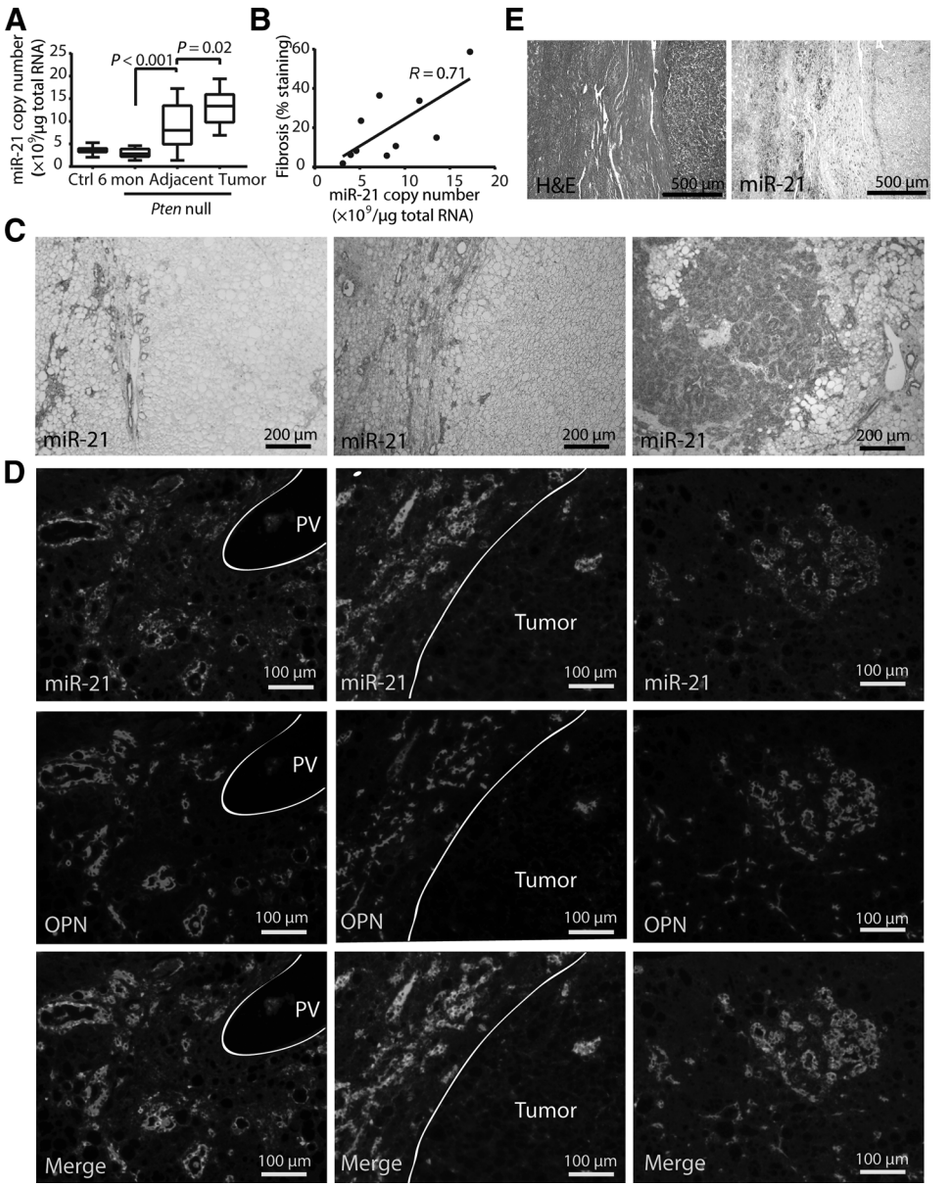

Figure 1.
miR-21 expression and cellular distribution in *Pten*-null mice. A, expression of miR-21 in liver from the *Pten*-null mice expressed as copies per μg of total RNA. B, correlation between miR-21 expression and liver fibrosis calculated using Pearson correlation analysis. C, miR-21 *in situ* hybridization: the dark-gray staining shows miR-21–positive cells present in areas of ductular reaction within the adjacent liver (left), surrounding the tumors (middle), and within cholangiolar tumors (right); magnification, ×100. D, immunofluorescence costaining of miR-21 and OPN in areas of ductular reaction within the adjacent liver (left), in areas surrounding the tumors (middle), and within cholangiolar hyperplasia (right); scale bar, 100 μm. E, H&E staining and miR-21 *in situ* hybridization of a representative human HCC showing miR-21 staining in areas surrounding the tumor and lack of staining in the tumor.

group identified the placebo tumors as displaying multiple morphologic characteristics, including HCC, cholangiocarcinoma, and hepatocholangiocellular carcinoma. In contrast, anti-miR-21 treated tumors showed a significant reduction in the incidence of cholangiolar tumors with incidence of cholangiocarcinoma and hepatocholangiocellular carcinoma decreasing from 29% and 71%, respectively, in the placebo treated group to 9% and 27%, respectively, in the anti-miR-21 treated group. In addition, anti-miR-21 treatment resulted in a decrease in the grade of tumor malignancy from predominantly pleomorphic and heterogeneic HCC to well-differentiated HCC. The incidence of pleomorphic HCC decreased from 42% in the placebo-treated group to 27% in the anti-miR-21 treated group. The majority of tumors in anti-miR-21 treated group were well differentiated HCCs, suggesting that inhibition of miR-21 resulted not only in reduced tumor growth, but also in histologically less malignant liver tumors. Representative images of hepatocholangiocellular carcinoma and pleomorphic HCC in the placebo-treated group and of well-differentiated HCC in the anti-miR-21 treated groups are shown in Supplementary Fig. S2.

Finally, because of the strong correlation we observed between liver fibrosis and miR-21 expression, we also evaluated the effects of anti-miR-21 treatment on fibrosis in adjacent liver tissue. Masson's trichrome staining showed a significant reduction of fibrosis from 19.0% to 12.0% ($P = 0.002$) upon anti-miR-21 treatment (Fig. 2E).

Anti-miR-21 treatment results in a significant reduction of progenitor cells and S100A4$^+$ cancer-associated stromal cells

To determine the mechanisms by which anti-miR-21 inhibits tumor growth and liver fibrosis, we first evaluated the effects of

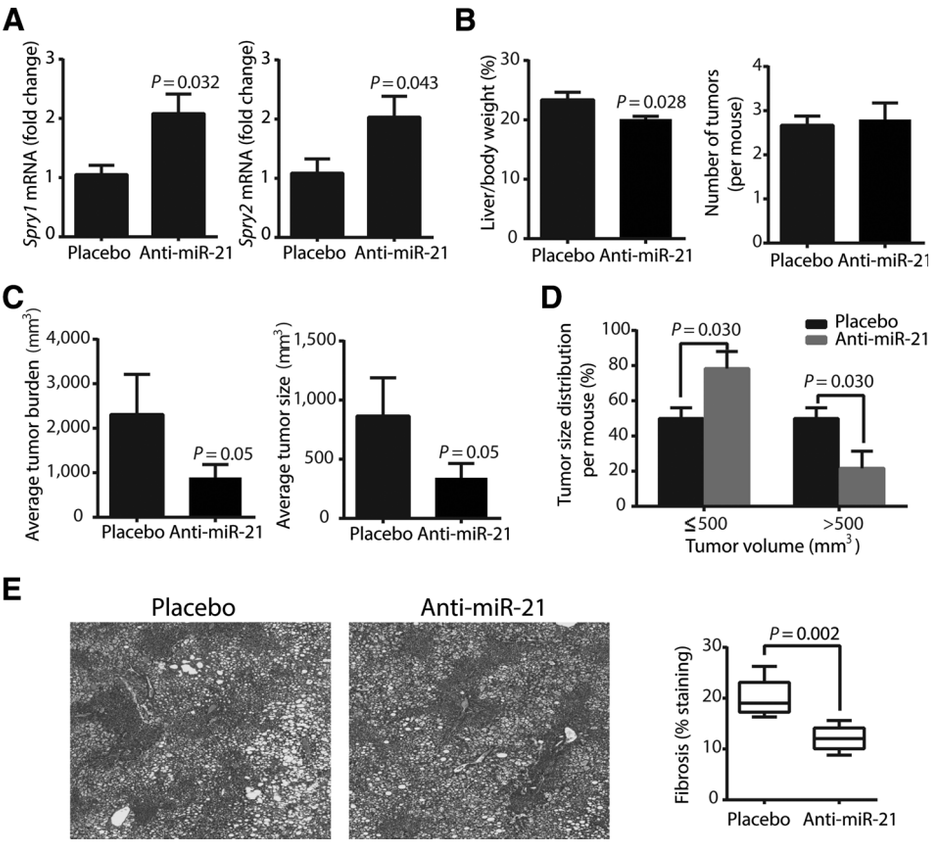

Figure 2.
Effect of anti-miR-21 treatment on tumor growth, tumor phenotype, and liver fibrosis. A, hepatic expression of miR-21 target genes, *Spry1* and *Spry2*, in placebo and anti-miR-21–treated mice ($n = 6$ mice per group) measured by qRT-PCR and shown as fold changes to the expression average in the placebo group. B, average liver/body weight ratio and number of tumors per mouse detected at necropsy. C, average tumor burden and tumor size per treatment group. D, tumor size distribution per mouse in each group. E, liver fibrosis measured by Masson's trichrome staining. Representative staining pictures (magnification, ×40) are shown together with quantification corresponding to the percentage of positive staining areas in each mouse.

anti-miR21 treatment on OPN-expressing progenitor cells. A strong reduction in OPN^+ cell population was observed following anti-miR-21 treatment. EPCAM, another marker of hepatic progenitor cells and biliary cells showed similar reduction. In addition, S100A4, a marker of cancer-associated stromal cells was also tested. Anti-miR-21 treatment resulted in a dramatic decrease of $S100A4^+$ cells (Fig. 3A). These results were further validated by real-time PCR confirming a significant decrease in *Opn and Epcam*

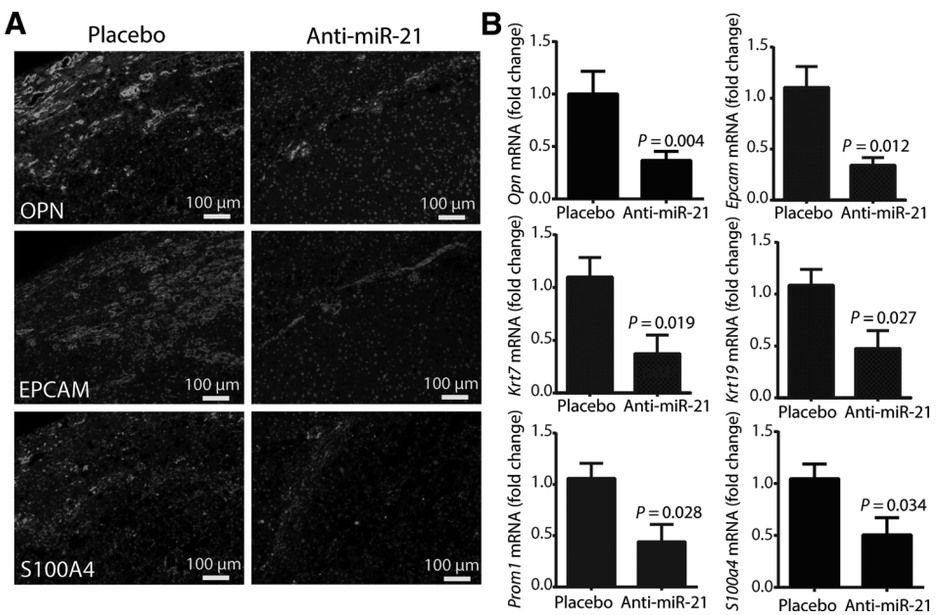

Figure 3.
Reduction in progenitor and $S100A4^+$ cell populations upon anti-miR-21 treatment. A, representative immunofluorescence tissue staining pictures (magnification, ×100) for OPN, EPCAM, and S100A4 in tumors of placebo and anti-miR-21–treated mice. B, mRNA expression of *Opn*, *Epcam*, *Krt7*, *Krt19*, *Prom1*, and *S100a4* measured by qRT-PCR in tumors of both treatment groups.

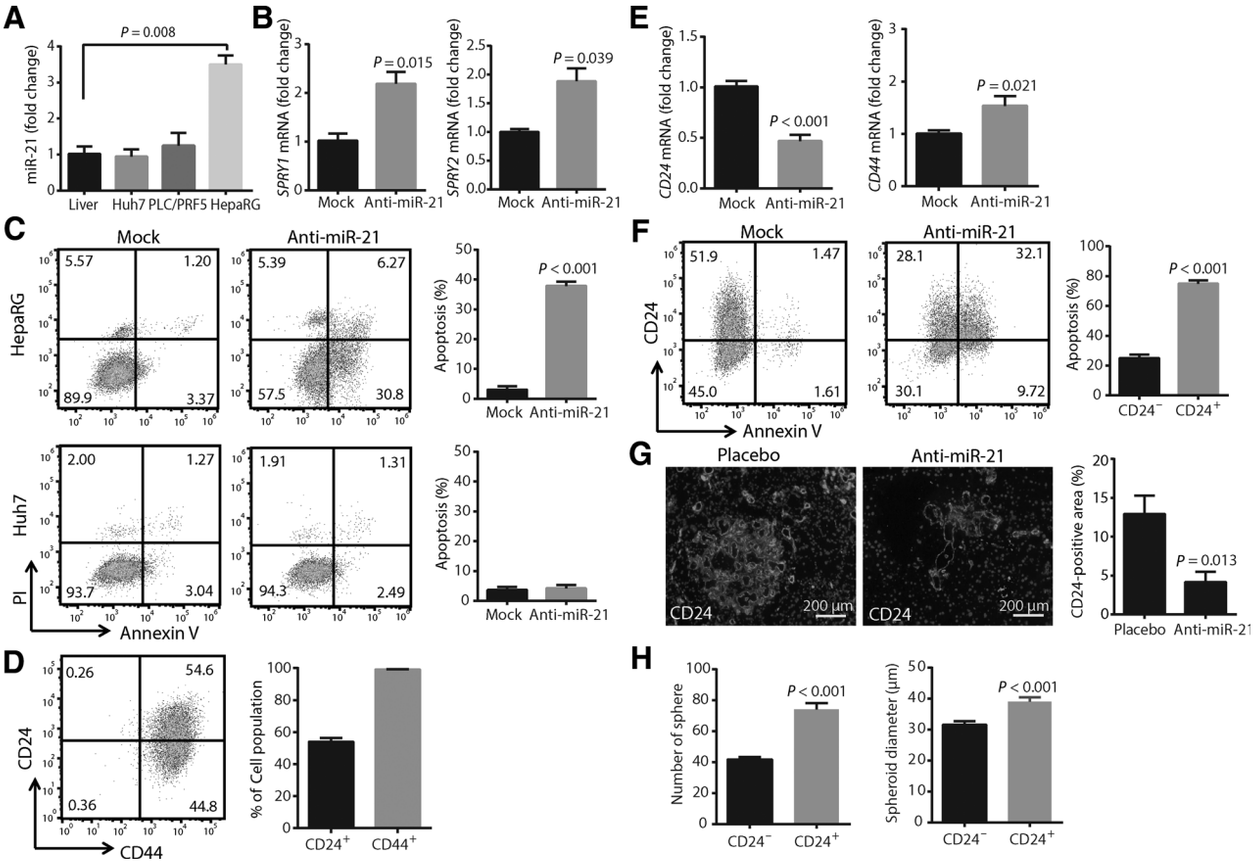

Figure 4.

Apoptosis of CD24$^+$ cells following anti-miR-21 treatment. A, miR-21 levels in healthy liver, hepatoma cell lines Huh7 and PLC/PRF5, and liver progenitor HepaRG cells. B, expression of miR-21 target genes, *SPRY1* and *SPRY2*, in HepaRG upon anti-miR-21 transfection. C, progenitor HepaRG cells and Huh7 hepatoma cells were transfected with 20 nmol/L anti-miR-21 oligonucleotide for 72 hours and costained with Annexin V and PI. Cell apoptosis was analyzed by flow cytometry. The right panel shows the quantification data from three independent experiments. D, HepaRG cells were stained with CD24 and CD44 antibodies and CD24$^+$ and CD44$^+$ cell populations were characterized by flow cytometry. The right panel shows the quantification data from three independent experiments. E, changes in *CD24* and *CD44* mRNA expression in HepaRG cells following anti-miR-21 transfection. F, HepaRG cells were transfected with anti-miR-21, costained with CD24 antibody and Annexin V, and then analyzed by flow cytometry. The right panel shows the quantification data from three independent experiments. G, reduction in CD24$^+$ progenitor cell population upon anti-miR-21 treatment of *Pten*-null mice shown with representative immunofluorescence tissue staining pictures for CD24 (magnification, ×100) and with quantification data calculated using the percentage of positive staining areas in liver from both treatment groups. H, quantification of spheres formed by CD24$^+$ and CD24- HepaRG cells.

mRNA expression (−2.7-fold; $P = 0.004$ and −2.9-fold; $P = 0.012$ respectively). The expression of other hepatic progenitor markers *Krt7*, *Krt19* and of the stem cell marker *Prom1* was also significantly reduced upon anti-miR-21 treatment (−2.7-fold; $P = 0.019$; −2.1-fold; $P = 0.027$ and −2.3-fold; $P = 0.028$, respectively). Finally, anti-miR-21 treatment resulted in a significant reduction of *S100a4* mRNA expression (−2.1-fold; $P = 0.034$; Fig. 3B). Together, these data showed that anti-miR-21 treatment results in a decrease in progenitor cell population, an effect accompanied with a decrease in S100A4$^+$ cancer-associated stromal cells.

MiR-21 is required for the survival of CD24$^+$ cells: a mechanism mediated by osteopontin and integrin αv

To determine the mechanisms by which anti-miR-21 results in a decrease in progenitor cell population, we treated the human HepaRG liver progenitor cells with 20 nmol/L anti-miR-21 oligonucleotide. miR-21 level was 3.5-fold higher in HepaRG cells compared with healthy liver and hepatoma cells lines Huh7 and PLC/PRF5 (Fig. 4A) and anti-miR-21 treatment resulted in increased expression of miR-21 targets, *SPRY1*, and *SPRY2* (2.2-fold; $P = 0.015$ and 1.9-fold; $P = 0.039$, respectively), validating the efficiency of the anti-miR-21 treatment in HepaRG cells (Fig. 4B). After 72 hours of anti-miR-21 treatment, an average of 38% of the HepaRG cells underwent apoptosis as shown by Annexin V/PI staining (Fig. 4C, top). The same treatment in the hepatoma Huh7 cells did not induce any apoptosis (Fig. 4C, bottom). To further identify the liver progenitor cell subpopulation undergoing apoptosis upon miR-21 inhibition, we stained HepaRG cells with antibodies directed against two commonly used liver stem cell surface markers CD44 and CD24. Approximately 54% of HepaRG cells expressed CD24, whereas 99% of HepaRG cells expressed CD44 (Fig. 4D). Upon miR-21 inhibition, *CD24* mRNA expression in HepaRG cells decreased (−2.13 fold; $P < 0.001$), whereas *CD44* mRNA expression slightly increased, suggesting a specific effect of miR-21 on CD24$^+$ cells (Fig. 4E). Costaining of CD24

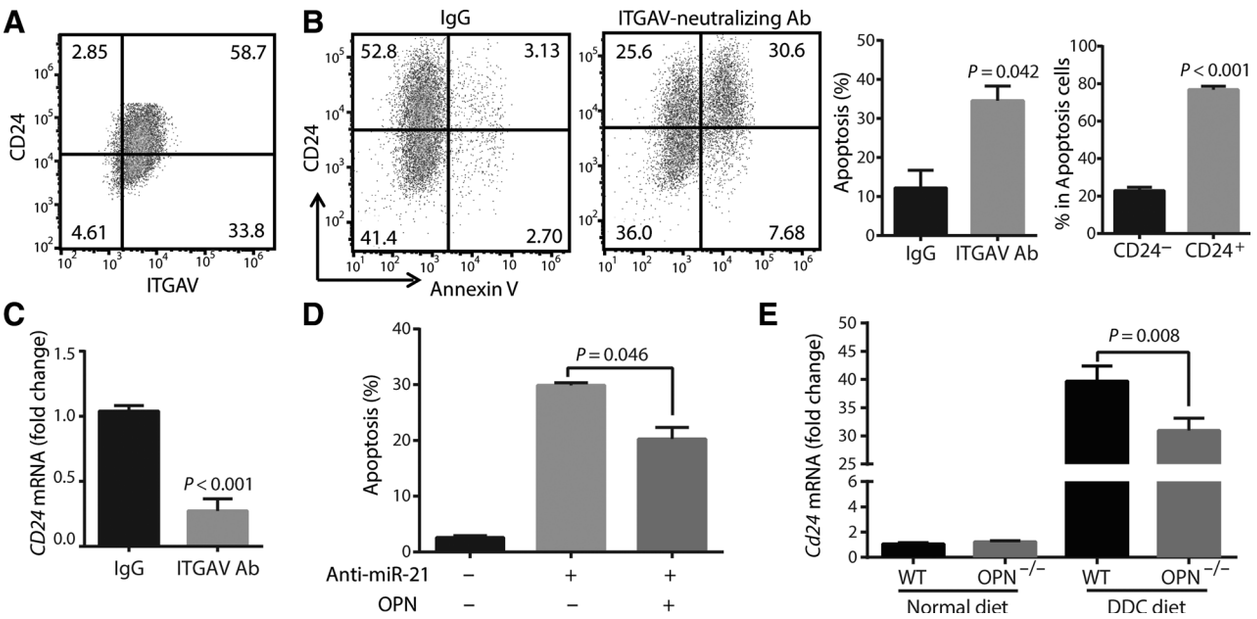

Figure 5.

Modulation of $CD24^+$ cell survival by OPN and ITGAV. A, HepaRG cells were costained with CD24 and ITGAV antibodies and the positive populations were characterized by flow cytometry. B, apoptosis of $CD24^+$ cell population upon treatment with neutralizing ITGAV antibody. Right, quantification data from three independent experiments, including percentage of apoptotic cells induced by ITGAV-neutralizing antibody treatment and the distribution of these apoptotic cells between $CD24^-$ and $CD24^+$ population. C, *CD24* mRNA expression upon ITGAV-neutralizing antibody treatment measured by qRT-PCR. D, HepaRG cells were treated with or without recombinant OPN protein (1 μg/mL) following anti-miR-21 transfection. Cell apoptosis was analyzed at 72 hours by costaining with Annexin V and PI. The figure shows the quantification data from three independent experiments. E, *Cd24* mRNA expression in liver from wt and $OPN^{-/-}$ mice treated for 4 weeks with DDC.

and Annexin V further showed that the large majority (75%) of apoptotic cells resulting from miR-21 inhibition were $CD24^+$ cells (Fig. 4F). The specific effect of miR-21 inhibition on the $CD24^+$ subpopulation of liver progenitor cells was further confirmed *in vivo*, by immunostaining showing a significant reduction of $CD24^+$ cells in *Pten*-null liver treated with anti-miR-21 from 12.9% to 4.1% ($P = 0.013$; Fig. 4G). In conclusion, miR-21 is required for the survival of $CD24^+$ liver stem cells. To further evaluate whether CD24 is indeed a stem-like marker, we separated HepaRG cells into $CD24^+$ and $CD24^-$ populations by FACS and subjected them to sphere formation assays. $CD24^+$ cells formed significantly larger spheres and at a significantly higher frequency as compared with $CD24^-$ cells (Fig. 4H).

We wished to identify the mediators of anti-miR-21 induced apoptosis of $CD24^+$ cells. We failed to identify candidate targets of miR-21 with apoptotic functions and preferential effects on $CD24^+$ cells. We therefore investigated the possible involvement of external signaling effects. We measured the expression of integrin αv (ITGAV), a receptor for OPN. Over 90% of HepaRG cells expressed ITGAV (Fig. 5A). To evaluate whether ITGAV signaling is required for $CD24^+$ cells survival, HepaRG cells were treated with 5 μg/mL ITGAV-neutralizing antibody for 72 hours. This treatment resulted in the apoptosis of 34.5% HepaRG cells. Among those apoptotic cells, 77% were $CD24^+$ cells (Fig. 5B). Real-time PCR also showed that ITGAV-neutralizing antibody treatment caused a strong (−3.7-fold; $P < 0.001$) decrease in *CD24* mRNA expression (Fig. 5C). We then added 1 μg/mL of recombinant OPN protein to the cell culture medium following anti-miR-21 transfection. Addition of OPN partially blocked the anti-miR-21 induced apoptosis of HepaRG cells, decreasing apoptosis from 29.87% to 20.25% ($P = 0.046$; Fig. 5D). Together, these results suggest that OPN is required for the survival of $CD24^+$ cells, an effect mediated by ITGAV. To further validate the role of OPN on $CD24^+$ cells survival, OPN knockout ($OPN^{-/-}$) mice were challenged with 4-week DDC diet, a classic liver injury model that strongly induces liver progenitor cell proliferation. DDC diet dramatically enhanced *Cd24* mRNA expression (39.7-fold) in wt mice. In $OPN^{-/-}$ mice, DDC-induced *Cd24* expression was significantly reduced ($P = 0.021$; Fig. 5E).

Inhibition of *Notch2* in *Pten*-null tumors upon anti-miR-21 treatment

To further identify the upstream events leading to OPN inhibition by anti-miR-21, we investigated whether *Notch* expression and activity were increased in *Pten*-null liver and tumors and whether anti-miR-21 treatment affected *Notch* expression and activity. The *Notch* family members have been associated with biliary differentiation of hepatoblast, liver carcinogenesis, and liver fibrosis. In addition, *Opn* expression is directly regulated by the transcriptional factor RUNX2, a *Notch* target. *Runx2* was significantly increased in *Pten*-null tumors compared with adjacent liver (1.5-fold, $P = 0.011$) and anti-miR-21 treatment resulted in a −1.5-fold reduction of *Runx2* mRNA in tumors ($P = 0.009$). Similarly, the expression of another *Notch* target, *Hes1* was increased in *Pten*-null tumor compared with adjacent liver (1.7-fold; $P = 0.019$) and strongly reduced upon anti-miR-21 treatment (−3.3-fold; $P < 0.001$; Fig. 6A). These results are indicative of increased *Notch* activity in *Pten*-null tumors that can be inhibited by anti-miR-21 treatment. We then measured the

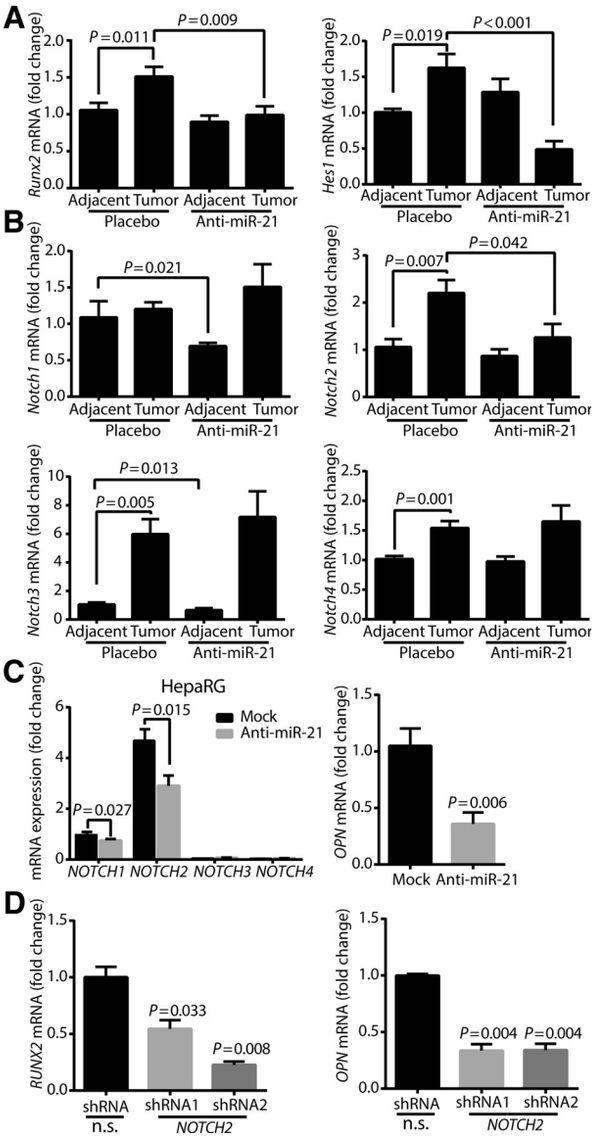

Figure 6.
Downregulation of *Notch* upon anti-miR-21 treatment *in vivo* and *in vitro*. A and B, *Runx2*, *Hes1*, *Notch1*, *Notch2*, *Notch3*, and *Notch4* mRNA expression measured by qRT-PCR in *Pten*-null tumors and adjacent liver. C, regulation of the *NOTCH* family members and *OPN* expression by anti-miR-21 treatment in HepaRG cells. D, *RUNX2* and *OPN* expression in HepaRG *NOTCH2* stable knocking down cell lines measured by qRT-PCR.

expression of *Notch 1*, *2*, *3* and *4*. Although the expression of *Notch1* was not increased in tumors compared with adjacent liver, the expression of *Notch2*, *Notch3*, and *Notch4* was significantly increased in tumors (2.2-fold; $P = 0.007$; 6.0-fold; $P = 0.005$; 1.5-fold; $P = 0.001$, respectively). Anti-miR-21 significantly reduced *Notch1* and *Notch3* expression in the liver ($P = 0.021$ and $P = 0.013$, respectively) but had no effect on their expression in tumors. In contrast, anti-miR-21 treatment resulted in a reduction of *Notch2* in tumors (−1.8 fold, $P = 0.042$). No effect of anti-miR-21 treatment on Notch4 was observed (Fig. 6B). Because anti-miR-21 targets hepatic progenitor cells, we evaluated whether *Notch2* was preferentially expressed in these cells. In HepaRG cells, *NOTCH2* is the major *NOTCH* gene, followed by *NOTCH1*. *NOTCH3* and *NOTCH4* mRNAs are expressed at very low levels. Anti-miR-21 treatment of HepaRG cells resulted in a concomitant decrease in *NOTCH2* and *OPN* expression (−1.6-fold; $P = 0.015$ and −2.8-fold; $P = 0.006$, respectively; Fig. 6C). We further showed that *NOTCH2* downregulation by shRNA in HepaRG cells resulted in *RUNX2* and *OPN* downregulation (Fig. 6D). Together, these results showed that *NOTCH2* is enriched in progenitor cells and mediates the downregulation of *OPN* by anti-miR-21 treatment.

Anti-miR-21 treatment prevents tumor development

Because of the effects of miR-21 inhibition on $CD24^+$ cell survival, OPN levels, expansion of $S100A4^+$ stromal cells, and *Notch* activity, we investigated whether targeting miR-21 could prevent tumor development *in vivo* in *Pten*-null mice. We treated 7.5-month-old *Pten*-null mice with anti-miR-21 for 6 weeks. Ultrasound did not detect any tumor in these mice at the start of treatment. At the end of treatment, the incidence of histologically confirmed tumors was 67% in the placebo-treated group and 33% in the anti-miR-21 treated group (Fig. 7A). The average tumor burden in anti-miR-21-treated mice was also significantly smaller than in mice from the placebo-treated group (23 mm^3 compared with 107 mm^3, $P = 0.039$; Fig. 7B). While the average volume of the largest tumor in mice from the placebo group was 92 mm^3, the average volume of the largest tumor in mice from the anti-miR-21 group was only 18 mm^3 ($P = 0.05$; Fig. 7C). Overall, only one tumor in the anti-miR-21 treated group was over 20 mm^3. Ultrasound analysis also showed that anti-miR-21 treatment significantly reduced the tumor growth rate from 2.24-fold to 1.25-fold over 14 days ($P = 0.029$; Fig. 7D). As observed in the first set of *Pten*-null–treated mice, fibrosis was significantly reduced from 14.3% to 7.2% ($P = 0.014$) upon anti-miR-21 treatment (Fig. 7E).

Discussion

MiR-21 has been identified as an onco-miR associated with many types of cancers, including HCC and intrahepatic cholangiocarcinoma (10, 19). miR-21 promotes cancer cell proliferation and invasion, and prevents apoptosis through the regulation of its target genes (8, 20, 21). The study presented here is the first evaluation of miR-21 as a therapeutic and preventive target in a genetically engineered mouse model of cancer. We found miR-21 expression in liver to be enriched in progenitor cells. Furthermore, we showed that a subpopulation of these progenitor cells, $CD24^+$ cells, is dependent on miR-21 for their survival, an effect mediated by OPN-ITGAV signaling, and that anti-miR-21 treatment reduced $CD24^+$ progenitor cell population *in vivo* by inhibiting RUNX2-mediated transcriptional regulation of OPN expression. $CD24^+$ cells have been identified as liver tumor-initiating cells and have been associated with higher risk of tumor recurrence (22). CD24 is an important molecule for stem cell self-renewal and tumor initiation ability through regulation of STAT3 phosphorylation and NANOG expression (22, 23). STAT3 can promote miR-21 expression by direct binding to the promoter region of miR-21 (24–27). It is therefore likely that the high expression of miR-21 in $CD24^+$ cells we observed is mediated by STAT3.

The reduction in tumor incidence and growth following anti-miR-21 treatment *in vivo* may be the direct consequence of the depletion of $CD24^+$ cell population. miR-21 may mediate the

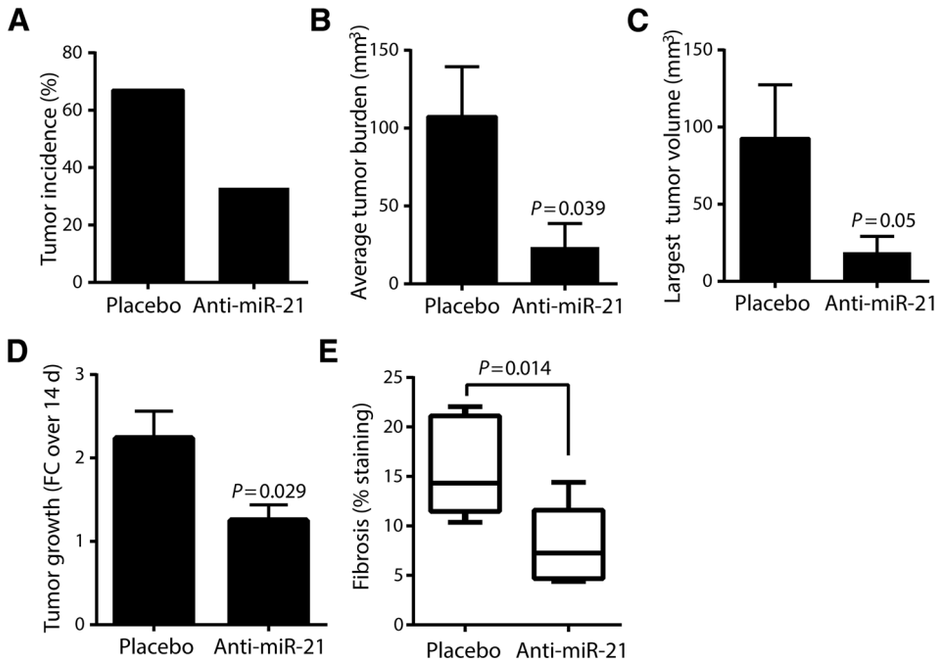

Figure 7.
Effect of anti-miR-21 treatment on liver fibrosis and tumor development. A–C, effects of anti-miR-21 treatment on tumor incidence (A), average tumor burden per mouse (B), and largest tumor volume per mouse (C). D, tumor growth expressed as fold change over 2 weeks of treatment, in placebo and anti-miR-21 treatment groups as determined by ultrasound. E, liver fibrosis measured by Masson's Trichrome staining.

early events in liver tumor initiation by maintaining the survival of $CD24^+$ liver tumor-initiating cells. This reduction in stem cell population may also explain the reduced malignancy of the tumors and concomitant increased differentiated phenotype following anti-miR-21 treatment. The increased differentiated phenotype following anti-miR-21 treatment may also result from the inhibition in *Notch* activity we observed. *Notch* signaling regulates biliary differentiation of hepatoblast in the developing and adult liver (28), drives cholangiocarcinoma development through trans-differentiation of hepatocytes (28–30), and contributes to liver carcinogenesis (31–33). *Notch* signaling has also been reported to modulate hepatic fibrosis (34). We found that *Notch2* is the main *Notch* family member expressed in *Pten*-null liver tumors. This preferential expression of *Notch2* may be due to the predominant expression of *Notch2* in $CD24^+$ progenitor cells. While anti-miR-21 treatment decreased *Notch1* expression in adjacent liver, *Notch2* expression decreased in tumors following anti-miR-21 treatment. This observation suggests that the different members of *Notch* have different cell distribution and nonredundant functions in liver.

The reduction in tumor incidence and growth following anti-miR-21 treatment *in vivo* may also be the direct consequence of a reduction in fibrosis and changes in the stroma largely associated with depletion of $S100A4^+$ and of $CD24^+$ cells, and reduction in OPN levels. A role for miR-21 in renal and cardiac fibrosis has been previously reported (1, 12, 35). Although miR-21 has been reported increased upon profibrogenic stimulation in liver (36), this is the first report demonstrating a direct role of miR-21 in liver fibrosis with a strong positive correlation between miR-21 levels and fibrosis severity in the *Pten*-null liver and a strong antifibrotic effect of anti-miR-21 treatment. In this model, we did not observe any correlation between α-SMA levels, a stellate cell marker and the effect of anti-miR-21 on fibrosis. Instead the expression of S100A4 decreased following anti-miR-21 treatment. This decrease was associated with a strong reduction of osteopontin, an extracellular matrix protein known to be involved in liver fibrosis and early stages of liver tumor development (37, 38). Crosstalk between $CD24^+$ cells and $S100A4^+$ cells may contribute to the extension of fibrosis in the liver and anti-miR-21 treatment may reduce liver fibrosis by blocking this crosstalk.

In summary, this study provides *in vivo* evidence of a role for miR-21 in maintaining the survival of $CD24^+$ progenitor cells and of a crosstalk between progenitor cells and cancer-associated stromal cells. It also suggests that anti-miR-21 may be effective at targeting tumor initiating cells as well as the tumor microenvironment, and therefore shows great promise for clinical studies of liver cancer prevention and treatment. The results of the study are summarized in a model diagram (Supplementary Fig. S3). Further study is warranted to determine whether anti-miR-21 treatment can be effective as a companion therapeutic agent to drugs killing the tumor cells or as a therapeutic target for the prevention of liver tumor in patients at risk and the prevention of recurrence.

Disclosure of Potential Conflicts of Interest

No potential conflicts of interest were disclosed.

Authors' Contributions

Conception and design: J. Zhang, S. Zabludoff, R. Kalluri, L. Beretta
Development of methodology: S. Cermelli, S. Zabludoff
Acquisition of data (provided animals, acquired and managed patients, provided facilities, etc.): J. Zhang, J. Jiao, S. Cermelli, K. Muir, A. Rashid, M. Gagea
Analysis and interpretation of data (e.g., statistical analysis, biostatistics, computational analysis): J. Zhang, K. Muir, M. Gagea, S. Zabludoff
Writing, review, and/or revision of the manuscript: J. Zhang, J. Jiao, A. Rashid, M. Gagea, S. Zabludoff, R. Kalluri, L. Beretta
Administrative, technical, or material support (i.e., reporting or organizing data, constructing databases): K. Muir, K.H. Jung, R. Zou
Study supervision: L. Beretta

Acknowledgments

The authors thank Drs. Eric Marcusson and Deidre MacKenna from Regulus Therapeutics for expert assistance with targeting miR-21 *in vivo*.

Grant Support

This work was supported in part by the MD Anderson Cancer Center Support Grant CA016672, through a Multidisciplinary Research Program Award.

The costs of publication of this article were defrayed in part by the payment of page charges. This article must therefore be hereby marked *advertisement* in accordance with 18 U.S.C. Section 1734 solely to indicate this fact.

Received April 23, 2014; revised January 13, 2015; accepted February 3, 2015; published OnlineFirst March 13, 2015.

References

1. Kumarswamy R, Volkmann I, Thum T. Regulation and function of miRNA-21 in health and disease. RNA Biol 2011;8:706–13.
2. Calin GA, Croce CM. MicroRNA signatures in human cancers. Nat Rev Cancer 2006;6:857–66.
3. Garzon R, Marcucci G, Croce CM. Targeting microRNAs in cancer: rationale, strategies and challenges. Nat Rev Drug Discov 2010;9:775–89.
4. Jiang J, Gusev Y, Aderca I, Mettler TA, Nagorney DM, Brackett DJ, et al. Association of MicroRNA expression in hepatocellular carcinomas with hepatitis infection, cirrhosis, and patient survival. Clin Cancer Res 2008; 14:419–27.
5. Ladeiro Y, Couchy G, Balabaud C, Bioulac-Sage P, Pelletier L, Rebouissou S, et al. MicroRNA profiling in hepatocellular tumors is associated with clinical features and oncogene/tumor suppressor gene mutations. Hepatology 2008;47:1955–63.
6. Burchard J, Zhang C, Liu AM, Poon RT, Lee NP, Wong KF, et al. microRNA-122 as a regulator of mitochondrial metabolic gene network in hepatocellular carcinoma. Mol Syst Biol 2010;6:402.
7. Sato F, Tsuchiya S, Meltzer SJ, Shimizu K. MicroRNAs and epigenetics. FEBS J 2011;278:1598–609.
8. Gramantieri L, Fornari F, Callegari E, Sabbioni S, Lanza G, Croce CM, et al. MicroRNA involvement in hepatocellular carcinoma. J Cell Mol Med 2008;12:2189–204.
9. Mizuguchi Y, Mishima T, Yokomuro S, Arima Y, Kawahigashi Y, Shigehara K, et al. Sequencing and bioinformatics-based analyses of the microRNA transcriptome in hepatitis B-related hepatocellular carcinoma. PLoS ONE 2011;6:e15304.
10. Karakatsanis A, Papaconstantinou I, Gazouli M, Lyberopoulou A, Polymeneas G, Voros D. Expression of microRNAs, miR-21, miR-31, miR-122, miR-145, miR-146a, miR-200c, miR-221, miR-222, and miR-223 in patients with hepatocellular carcinoma or intrahepatic cholangiocarcinoma and its prognostic significance. Mol Carcinog 2013;52:297–303.
11. Selaru FM, Olaru AV, Kan T, David S, Cheng Y, Mori Y, et al. MicroRNA-21 is overexpressed in human cholangiocarcinoma and regulates programmed cell death 4 and tissue inhibitor of metalloproteinase 3. Hepatology 2009;49:1595–601.
12. Thum T, Gross C, Fiedler J, Fischer T, Kissler S, Bussen M, et al. MicroRNA-21 contributes to myocardial disease by stimulating MAP kinase signalling in fibroblasts. Nature 2008;456:980–4.
13. Liu G, Friggeri A, Yang Y, Milosevic J, Ding Q, Thannickal VJ, et al. miR-21 mediates fibrogenic activation of pulmonary fibroblasts and lung fibrosis. J Exp Med 2010;207:1589–97.
14. Marquez RT, Bandyopadhyay S, Wendlandt EB, Keck K, Hoffer BA, Icardi MS, et al. Correlation between microRNA expression levels and clinical parameters associated with chronic hepatitis C viral infection in humans. Lab Invest 2010;90:1727–36.
15. El-Serag HB, Rudolph KL. Hepatocellular carcinoma: epidemiology and molecular carcinogenesis. Gastroenterology 2007;132:2557–76.
16. Horie Y, Suzuki A, Kataoka E, Sasaki T, Hamada K, Sasaki J, et al. Hepatocyte-specific Pten deficiency results in steatohepatitis and hepatocellular carcinomas. J Clin Invest 2004;113:1774–83.
17. Stiles B, Wang Y, Stahl A, Bassilian S, Lee WP, Kim YJ, et al. Liver-specific deletion of negative regulator Pten results in fatty liver and insulin hypersensitivity [corrected]. Proc Natl Acad Sci U S A 2004;101:2082–7.
18. Yu RZ, Lemonidis KM, Graham MJ, Matson JE, Crooke RM, Tribble DL, et al. Cross-species comparison of *in vivo* PK/PD relationships for second-generation antisense oligonucleotides targeting apolipoprotein B-100. Biochem Pharmacol 2009;77:910–9.
19. Xu J, Wu C, Che X, Wang L, Yu D, Zhang T, et al. Circulating microRNAs, miR-21, miR-122, and miR-223, in patients with hepatocellular carcinoma or chronic hepatitis. Mol Carcinog 2011;50:136–42.
20. Meng F, Henson R, Wehbe-Janek H, Ghoshal K, Jacob ST, Patel T. MicroRNA-21 regulates expression of the PTEN tumor suppressor gene in human hepatocellular cancer. Gastroenterology 2007;133: 647–58.
21. Zhou L, Yang ZX, Song WJ, Li QJ, Yang F, Wang DS, et al. MicroRNA-21 regulates the migration and invasion of a stem-like population in hepatocellular carcinoma. Int J Oncol 2013;43:661–9.
22. Lee TK, Castilho A, Cheung VC, Tang KH, Ma S, Ng IO. CD24(+) liver tumor-initiating cells drive self-renewal and tumor initiation through STAT3-mediated NANOG regulation. Cell Stem Cell 2011; 9:50–63.
23. Liu AY, Cai Y, Mao Y, Lin Y, Zheng H, Wu T, et al. Twist2 promotes self-renewal of liver cancer stem-like cells by regulating CD24. Carcinogenesis 2014;35:537–45.
24. Bourguignon LY, Earle C, Wong G, Spevak CC, Krueger K. Stem cell marker (Nanog) and Stat-3 signaling promote MicroRNA-21 expression and chemoresistance in hyaluronan/CD44-activated head and neck squamous cell carcinoma cells. Oncogene 2012;31:149–60.
25. Kohanbash G, Okada H. MicroRNAs and STAT interplay. Semin Cancer Biol 2012;22:70–5.
26. Loffler D, Brocke-Heidrich K, Pfeifer G, Stocsits C, Hackermuller J, Kretzschmar AK, et al. Interleukin-6 dependent survival of multiple myeloma cells involves the Stat3-mediated induction of microRNA-21 through a highly conserved enhancer. Blood 2007;110:1330–3.
27. Yang CH, Yue J, Fan M, Pfeffer LM. IFN induces miR-21 through a signal transducer and activator of transcription 3-dependent pathway as a suppressive negative feedback on IFN-induced apoptosis. Cancer Res 2010;70:8108–16.
28. Jeliazkova P, Jors S, Lee M, Zimber-Strobl U, Ferrer J, Schmid RM, et al. Canonical Notch2 signaling determines biliary cell fates of embryonic hepatoblasts and adult hepatocytes independent of Hes1. Hepatology 2013;57:2469–79.
29. Sekiya S, Suzuki A. Intrahepatic cholangiocarcinoma can arise from Notch-mediated conversion of hepatocytes. J Clin Invest 2012;122:3914–8.
30. Fan B, Malato Y, Calvisi DF, Naqvi S, Razumilava N, Ribback S, et al. Cholangiocarcinomas can originate from hepatocytes in mice. J Clin Invest 2012;122:2911–5.
31. Dill MT, Tornillo L, Fritzius T, Terracciano L, Semela D, Bettler B, et al. Constitutive Notch2 signaling induces hepatic tumors in mice. Hepatology 2013;57:1607–19.
32. Razumilava N, Gores GJ. Notch-driven carcinogenesis: The merging of hepatocellular cancer and cholangiocarcinoma into a common molecular liver cancer subtype. J Hepatol 2013;58:1244–5.
33. Villanueva A, Alsinet C, Yanger K, Hoshida Y, Zong Y, Toffanin S, et al. Notch signaling is activated in human hepatocellular carcinoma and induces tumor formation in mice. Gastroenterology 2012;143: 1660–9 e7.
34. Chen Y ZS, Qi D, Zheng S, Guo J, Zhang S, Weng Z. Inhibition of Notch signaling by a γ-secretase inhibitor attenuates hepatic fibrosis in rats. PLoS ONE 2013;7:11.
35. He Y, Huang C, Li J. miR-21 is a critical therapeutic target for renal fibrosis. Cell Biochem Biophys 2014;68:635–6.
36. Noetel A, Kwiecinski M, Elfimova N, Huang J, Odenthal M. microRNA are central players in anti- and profibrotic gene regulation during liver fibrosis. Front Physiol 2012;3:49.
37. Nagoshi S. Osteopontin: Versatile modulator of liver diseases. Hepatol Res 2014;44:22–30.
38. Shang S, Plymoth A, Ge S, Feng Z, Rosen HR, Sangrajrang S, et al. Identification of osteopontin as a novel marker for early hepatocellular carcinoma. Hepatology 2012;55:483–90.